14.6. THE IMPACTS OF MICROPHYSICS AND PLANETARY BOUNDARY LAYER PHYSICS ON MODEL SIMULATIONS OF U.S. DEEP SOUTH SUMMER CONVECTION

Eugene W. McCaul, Jr.[1], Jonathan L. Case[2], Bradley Zavodsky[3],
Jayanthi Srikishen[1], Jeffrey Medlin[4], and Lance Wood[5]
1. Universities Space Research Association, Huntsville, AL
2. ENSCO, Inc., and NASA SPoRT Center, Huntsville, AL
3. NASA SPoRT Center, Huntsville, AL
4. NOAA/NWS, Mobile, AL
5. NOAA/NWS, Houston, TX

1. INTRODUCTION

Convection-allowing numerical weather simulations have often been shown to produce convective storms that have significant sensitivity to choices of model physical parameterizations. Among the most important of these sensitivities are those related to cloud microphysics, but planetary boundary layer parameterizations also have a significant impact on the evolution of the convection. Aspects of the simulated convection that display sensitivity to these physics schemes include updraft size and intensity, simulated radar reflectivity, timing and placement of storm initiation and decay, total storm rainfall, and other storm features derived from storm structure and hydrometeor fields, such as predicted lightning flash rates.

In addition to the basic parameters listed above, the simulated storms may also exhibit sensitivity to imposed initial conditions, such as the fields of soil temperature and moisture, vegetation cover and health, and sea and lake water surface temperatures. Some of these sensitivities may rival those of the basic physics sensitivities mentioned earlier. These sensitivities have the potential to disrupt the accuracy of short-term forecast simulations of convective storms, and thereby pose significant difficulties for weather forecasters.

To make a systematic study of the quantitative impacts of each of these sensitivities, a matrix of simulations has been performed using all combinations of eight separate microphysics schemes, three boundary layer schemes, and two sets of initial conditions. The first version of initial conditions consists of the default data from large-scale operational model fields, while the second features specialized higher- resolution soil conditions, vegetation conditions and water surface temperatures derived from datasets created at NASA's Short-term Prediction and Operational Research Transition (SPoRT) Center at the National Space Science and Technology Center (NSSTC) in Huntsville, AL. Simulations as outlined above, each 48 in number, were conducted for five midsummer weakly sheared coastal convective events each at two sites, Mobile, AL (MOB) and Houston, TX (HGX). Of special interest to operational forecasters at MOB and HGX were accuracy of timing and placement of convective storm initiation, reflectivity magnitudes and coverage, rainfall and inferred lightning threat.

*Corresponding author address: Eugene W. McCaul, Jr., Universities Space Research Association, 320 Sparkman Drive Huntsville, AL 35805, e-mail: emccaul@usra.edu

2. DATA AND METHODOLOGY

The NWP model used in this study is the Weather Research and Forecasting (WRF) model, version 3.4.1, invoking the Advanced Research WRF dynamical core. The WRF model was executed using two nested grids covering areas centered on either MOB or HGX. The outer grid used a 9-km mesh with convection parameterized by the Kain-Fritsch cumulus scheme, while the inner 3-km grid used explicit convection. Besides the Kain-Fritsch scheme on the outer grid, other physical parameterization schemes held fixed in this study include the Dudhia shortwave radiation, RRTM longwave radiation, and Noah land surface model, all of which are documented in Skamarock et al. (2008). Each WRF run is configured with 40 standard sigma-pressure vertical layers, on a stretched grid with a 50-mb domain top. For each of five case dates in the summer of 2012 at both MOB and HGX, a matrix of 24 WRF simulations (8 distinct microphysics choices paired with 3 distinct boundary layer physics choices) was executed twice, once with default WRF conditions ("control" runs), and again with more detailed SPoRT data ("SPoRT" runs). In the control runs, the model used static fields and initial and boundary condition inputs supplied by the NCEP Global Forecast System (GFS) model 3-hourly forecasts, while the SPoRT runs utilized SPoRT-generated surface data obtained from the NASA Land Information System (LIS) offline integration of the Noah land surface model on a 3-km grid mesh (Case and White 2014), along with real-time 1-km MODIS green vegetation fraction (GVF; Case et al. 2014) projected onto a 4-km grid, and 2-km sea surface temperature composites (Case et al. 2012). The latter datasets are maintained at NASA's SPoRT Center and are produced in real-time for use in local NWP applications at many NOAA/NWS forecast offices. Each simulation was launched at 0600 UTC, during the diurnal minimum of convective activity, and was run for 24 h using 0-24 hour forecasts from the 0600 UTC cycle of the GFS model for initial and boundary conditions.

Maps of the outer and inner domains for MOB are given in Fig. 1. The domains for HGX are constructed in an analogous manner.

Weakly sheared summertime convection cases were selected for study, because they are especially challenging for forecasters. As both MOB and HGX are situated near the Gulf coast, sea breezes often serve as the trigger for deep convection there, and the location, timing and intensity of the weakly sheared convection can be difficult to forecast.

Hourly plots of a multitude of basic and derived model output fields were examined to assess the performance of each WRF configuration in terms of accuracy of the simulated timing, location and character of the forecast convection. Parameters studied included peak mid-level updraft speeds, composite reflectivities, location and timing of storm development, total storm rainfall, and peak lightning flash rate densities inferred from the WRF Lightning Forecast Algorithm (LFA; McCaul et al. 2009, McCaul et al. 2013). Reflectivities within the simulations were computed using the default WRF method, without customized embellishments for any of the microphysics schemes; although such embellishments were recommended for some schemes, the custom WRF-supplied software tended to produce unreliable results for reflectivity, and was thus abandoned in favor of the default software. The eight microphysics and three boundary layer schemes used in the simulation matrices are listed in Table 1. Microphysics schemes ranged from the legacy WRF Single Moment 6-species (WSM-6) scheme up through the more recent and sophisticated NSSL double moment scheme. The quasi-double moment Thompson scheme is also included, so that insights into its relative performance in operational forecasts by such as the High-Resolution Rapid Refresh (HRRR) WRF model can be examined. Microphysics schemes include WSM-6, Lin (LIN), Goddard (GOD), WRF Double Moment-6 Species (WDM-6), Thompson (THOM), Morrison (MORR), Milbrandt-Yau (MIL), and NSSL. Local mixing planetary boundary layer (PBL) schemes used included Mellor-Yamada-Janjic (MYJ), Quasi-Normal Scale Elimination (QNSE) and the Mellor-Yamada-Nakaniishi-Niino (MYNN).

Model output was compared both subjectively and objectively with radar-derived reflectivity data, and with rainfall data inferred from a combination of radar and rain gage data. For reflectivity, objective comparisons were made of the peak reflectivities seen in any of the simulations versus the peak observed values. For rainfall, patterns and amounts were scored against rainfall observations using the NCAR Model Evaluation Tools (MET) verification package. In the latter case, statistics such as time-dependent Heidke Skill Scores (HSS) were computed so that the rainfall performance of the various simulations could be determined in comparison to observations. Frequency of occurrence of gridpoints experiencing rainfall accumulations greater than a series of threshold amounts was also tallied, so that areal coverage biases in the various simulations could be documented. Peak 24-h rainfall accumulations in the simulations were also compared to peak values seen in the observations. To evaluate computational efficiency of the various WRF configurations, model run times for all the simulations were also tabulated, since run-time performance can have implications for the practicality of running certain configurations at NOAA/NWS forecast offices with limited computational capabilities.

For evaluating the possible lightning activity in the simulated storms, the LFA, a simple diagnostic method for making quantitative estimates of total lightning flash rate densities (FRDs) in simulated storms was also applied, so that relative variations in the inferred lightning could be examined across all physics combinations. The WRF LFA considers two main simulated variables, the upward graupel flux (GFX) in the mixed phase layer, which dictates the amplitude of the FRD estimates, and the total vertical ice integral (VII), which provides input regarding lightning threat footprint, as proxies for total lightning FRDs. For GFX, the layer with temperature of -15C is taken as the mixed phase layer. Both proxies have been found in global observational studies (Petersen et al. 2005; Cecil et al. 2005; Deierling and Peterson 2008) to be strongly related to storm flash rates. In McCaul et al. (2009), the peak values of the two simulated proxies in convective events in the Tennessee Valley area were found to be linearly related to the peak total lightning flash origin densities observed by the North Alabama Lightning Mapping Array (Goodman et al. 2005; Krehbiel et al. 2000). In the LFA, the GFX proxy serves to define the amplitudes of FRD, but is blended with the more widely distributed VII field to enhance the areal coverage accuracy of the lightning threat, as described by lightning flash extent density. The LFA strives to produce fields of total lightning threat that exhibit peak FRDs that match those of the strongest storms in a convective event. The LFA-derived peak FRD values were examined herein primarily for the purpose of intercomparisons of performances of the various physics scheme choices against the original WSM-6 design of the LFA; direct comparisons with any possible LMA observations were not feasible.

3. RESULTS AND DISCUSSION

Inspection of the simulation output reveals considerable sensitivity and complexity in the convective response to the choices of microphysics and boundary layer parameterizations, and especially to input soil moisture, GVF, and sea surface temperature. As a general rule, it is found that for the dry summer of 2012, use of the detailed and generally drier soil moisture data from the SPoRT LIS-Noah datasets resulted in simulations that produced less convective rainfall than in the "control" simulations. The dryness of the SPoRT simulations is statistically advantageous for days having

large amounts of convective rainfall, which the "control" WRF runs tend to overdo. Such wet days were more common in 2012 among the MOB cases than the HGX cases.

(a) 3 July 2012 case for MOB

An example is shown in Fig. 2a(top) for 24-h total rainfall from 3 July 2012 from MOB, for the full set of 24 "control" simulations. In Fig. 2b (bottom) is shown the full set of SPoRT-initialized simulations. Stage IV radar plus rain gage 24-h rainfall estimates (Lin and Mitchell 2005; Lin et al. 2005) for the 3 July case are shown in Fig. 2c. Time-evolving HSS values for the various QNSE schemes in the "control" and "SPoRT" simulations are provided in Fig. 3a-b (top and bottom, respectively). QNSE results are presented, as QNSE was found to be the best-performing PBL scheme in many instances. Note the general improvement in HSS values for the drier SPoRT runs, which is typical of what is seen in "wet" events at MOB in 2012. Part of the reason for the higher HSS scores in the SPoRT runs lies in the fact that, in those runs, the convection initiates northeast of MOB, consistent with radar data, rather than northwest of MOB, as in most of the control runs. For the usually drier HGX cases, the SPoRT initializations typically produced too little precipitation, often so much so that HSS scores were adversely affected for the SPoRT runs. An example of this is shown in Fig. 4a-b (top and bottom, respectively) for the QNSE runs. Note that the NSSL double-moment microphysics scheme appears to yield higher HSS values in many cases. This NSSL microphysics advantage was also commonly seen for PBL schemes other than QNSE (not shown).

Peak cumulative 24-h rainfall amounts from the "control" simulations for MOB on 3 July 2012 revealed considerable variability, with the greatest peak rainfall being 167.91 mm from the LIN/MYJ simulation, and the smallest being 88.76 mm from GOD/MYJ. The MYJ schemes have the largest mean peak 24-h rainfall amounts, while MYNN has the smallest. Stage IV estimates of peak rainfall for this event reached only 70.13 mm, which indicates the extent of rainfall overprediction in the "control" simulations. For all PBL schemes, the Lin microphysics produces the largest rainfall. The relative sensitivity of peak rainfall amounts, as measured by the range of peak FRD values divided by their mean, is largest for the MYJ simulations. The "SPoRT" simulations also exhibited much variability, but with smaller mean values, closer in line with observations. The largest peak rainfall was 139.95 mm from LIN/MYJ, while the smallest was 52.28 (GOD/QNSE). The QNSE PBL scheme yielded the smallest mean of peak rainfall amounts, while MYJ yielded the largest. Relative variability of rainfall across microphysics choices was largest for the QNSE simulations, which also produced the least rainfall, on average. For the SPoRT runs, the smallest peak rainfall variability across microphysics schemes was seen with MYJ PBL physics, contrary to what was seen in the "control" runs.

In terms of reflectivity in the "control" simulations, peak composite reflectivity reached 65.70 dBZ in THOM/MYJ, 60.44 in WDM-6/QNSE, and 62.97 in THOM/MYNN. The smallest peak reflectivities in each PBL series were 56-57 dBZ. Radar observations indicate that the true peak reflectivities were just above 65 dBZ, suggesting an advantage for Thompson/MYJ, and that the calculated reflectivities for almost all schemes are too small. This maximum in THOM/MYJ reflectivity performance is not matched, however, for LFA lightning FRDs, nor maximum 24-h precipitation.

Peak simulated values for the SPoRT MYJ runs were 60.84 (NSSL), with 61.19 (THOM) for SPoRT QNSE runs, and 60.79 (THOM) for SPoRT MYNN runs. In addition to peak reflectivities, the means of the maximum values of reflectivity were also slightly reduced in the SPoRT runs.

(b) LFA Analysis for 3 July 2012 MOB case

Lightning flash rate forecasts from the WRF LFA also exhibited much sensitivity to physics choices within the 24-simulation ensembles. For the 3 July 2012 MOB "control" cases, it is found, for example, that the greatest peak FRD, 24.05 flashes per sq. km/(5 min), is produced by the LIN/QNSE scheme, while the least, 7.91, is produced by the GODD/MYNN scheme. The default microphysics used in the original LFA design, WSM-6, yielded a peak of 15.89 flashes per sq. km/(5 min) in QNSE, but 14.87 and 12.13 in MYJ and MYNN PBL runs, respectively. Meanwhile, the quasi-double moment Thompson scheme as used in the HRRR model, yielded peak FRD values of 12.54, 11.38, and 9.50 for the MYJ, QNSE and MYNN PBL schemes. The HRRR actually employs the MYNN PBL scheme, so that it is suggested that HRRR LFA-derived FRD values in this case underestimate those from WSM-6 by a factor of $0.60 = 9.50/15.89$. Since the LFA is based on a simple linear relationship between GFX and FRD, recalibration of HRRR FRD values to be consistent with those from WSM-6 should require a simple magnification by the factor 1.67. QNSE runs featured the largest mean values of peak FRD, while MYNN produced the least. The MYNN results also displayed, by a small margin, the largest amount of relative sensitivity across the 8 microphysics runs.

As expected, the corresponding peak FRD values in the drier "SPoRT" runs were reduced relative to the "control" runs. The greatest peak FRD was 9.46 for WSM-6/MYNN, while the least was 2.17 for NSSL/QNSE. The three WSM-6 peak FRD values were 8.10, 5.14 and 9.46, for MYJ, QNSE and MYNN, respectively. For the Thompson scheme, peak FRD values were 4.49, 5.86 and 4.48, respectively. The QNSE runs exhibited the smallest mean peak FRD values, but the largest relative variability.

(c) Computational resource considerations

Computational efficiency is also a practical consideration for use of the various physics and initialization schemes. Inspection of run-time data from the simulations here (Fig. 5, results only from "control" simulations; "SPoRT" runs are similar) shows a clear tendency for simple schemes such as WSM-6/MYJ to run most quickly, while more elaborate schemes such as NSSL/QNSE can take nearly twice as much time to execute. The tradeoffs are not simple, as it was often the case that the more expensive scheme combinations turned in the best performances in terms of HSS. There are thus no obvious "best buy" recommendations, especially when computational resources are limited, as is often the case at NWS forecast offices running local model simulations.

4. SUMMARY AND FUTURE WORK

This paper presents an analysis of a multi-physics combination matrix for weakly-sheared summertime convective events over the U.S. Deep South. A matrix of simulations was made for both a control configuration using only GFS model initial and boundary conditions, and an experimental configuration using higher-resolution input land surface fields, GVF, and SST from SPoRT-generated datasets. In general, the input drier soil moisture provided by the SPoRT-LIS yielded an overall reduction in precipitation coverage which improved verification scores in "wet" cases, but degraded verification scores in "dry" case with more sparsely-distributed convection. While the matrix of PBL and microphysical schemes yielded variability in the space-time evolution of convection, it appears that the input SPoRT surface datasets often had an overall greater impact on the evolution of environmental conditions leading up to convective development.

Future work will involve examining in greater detail the additional 4 MOB and 5 HGX case studies to formulate more robust conclusions about the overall impact of SPoRT surface datasets and its interaction with different combinations of PBL and microphysics schemes in the WRF model. These additional cases will also help to improve the understanding of WRF LFA behavior in the HRRR model, based on the comparison between the WSM-6/MYJ in the original LFA calibration and the THOM/MYNN configuration in the current HRRR configuration.

5. ACKNOWLEDGMENTS

This research was funded by NASA's Short Term Prediction and Research Transition (SPoRT) project at Marshall Space Flight Center, and also by a Risk Reduction grant from the National Oceanic and Atmospheric Administration to Project 68, which involves studies of the WRF Lightning Forecast Algorithm in support of the planned launch of the Geostationary Lightning Mapper (GLM) on the GOES-R satellite platform.

6. REFERENCES

Case, J. L., F. J. LaFontaine, J. R. Bell, G. J. Jedlovec, S. V. Kumar, and C. D. Peters-Lidard, 2014: A real-time MODIS vegetation product for land surface and numerical weather prediction models. *Trans. Geosci. Remote Sens.*, **52(3)**, 1772–1786.

Case, J. L., F. J. LaFontaine, A. L. Molthan, B. T. Zavodsky, and R. A. Rozumalski, 2012: Recent upgrades to NASA SPoRT initialization datasets for the Environmental Modeling System. *Preprints*, 37th Natl. Wea. Assoc. Annual Meeting, Madison, WI, Natl. Wea. Assoc., P1.40.

Case, J. L., and K. D. White, 2014: Expansion of the real-time SPoRT-Land Information System for NOAA/National Weather Service situational awareness and local modeling applications. *Preprints*, 22nd Conf. on Num. Wea. Prediction / 26th Conf. on Wea. Analysis Forecasting, Atlanta, GA, Amer. Meteor. Soc., P162.

Cecil, D. J., S. J. Goodman, D. J. Boccippio, E. J. Zipser, and S. W. Nesbitt, 2005: Three years of TRMM precipitation features. Part I: Radar, radiometric, and lightning characteristics. *Mon. Wea. Rev.*, **133**, 543–566.

Deierling, W., and W. A. Petersen, 2008: Total lightning activity as an indicator of updraft characteristics. *J. Geophys. Res.*, *113*, D16210, doi: 10.1029/2007JD009598.

Goodman, S. J., R. Blakeslee, H. Christian, W. Koshak, J. Bailey, J. Hall, E. McCaul, D. Buechler, C. Darden, J. Burks, T. Bradshaw, and P. Gatlin, 2005: The North Alabama Lightning Mapping Array: Recent severe storm observations and future prospects. *Atmos. Res.*, **76**, 423–437.

Kain, J. S., S. R. Dembek, S. J. Weiss, J. L. Case, J. J. Levitt, and R. A. Sobash, 2010: Extracting unique information from high-resolution forecast models: Monitoring selected fields and phenomena every time step. *Wea. Forecasting*, **25**, 1536–1542.

Krehbiel, P.R., R.J. Thomas, W. Rison, T. Hamlin, J. Harlin, and M. Davis, 2000: GPS-based mapping system reveals lightning inside storms. *Eos*, **81**, 21–25.

Lin, Y., and K. E. Mitchell, 2005: The NCEP Stage II/IV hourly precipitation analyses: Development and applications. *Preprints*, 19th Conf. Hydrol, San Diego, CA, Amer. Meteor. Soc., 1.2.

Lin, Y., K. E. Mitchell, E. Rogers, and G. J. DiMego, 2005: Using hourly and daily precipitation analyses to improve model water budget. *Preprints*, Ninth Symp. on Integrated Observing and Assimilation Systems for the Atmosphere, Oceans, and Land Surface, San Diego, CA, Amer. Meteor. Soc., 3.3.

Lojou, J.-Y., and K. L. Cummins, 2005: On the representation of two- and three-dimensional total lightning information. *Preprints CD-ROM*, 1st Conf. Meteorol. Appl. Lightning Data, San Diego, CA, Amer. Meteor. Soc., paper 2.4.

Mansell, E. R, D. R. MacGorman, C. L. Ziegler, and J. M. Straka, 2002: Simulated three-dimensional

branched lightning in a numerical thunderstorm model. *J. Geophys. Res.*, *107*, 4075, doi: 10.1029/2000JD000244.

Mansell, E. R, D. R. MacGorman, C. L. Ziegler, and J. M. Straka, 2005: Charge structure and lightning sensitivity in a simulated multicell thunderstorm. *J. Geophys. Res.*, *110*, D12101, doi: 10.1029/2004JD005287.

McCaul, E. W., Jr., S. J. Goodman, K. M. LaCasse, and D. J. Cecil, 2009: Forecasting lightning threat using cloud-resolving model simulations. *Wea. Forecasting*, **24**, 709–729. (highlighted as a Paper of Note in *Bull. Amer. Meteorol. Soc.*, **90**, 772.)

Murphy, M. J., and N. Demetriades, 2005: An analysis of lightning holes in a DFW supercell storm using total lightning and radar information. *Preprints CD-ROM*, 1st Conf. Meteorol. Appl. Lightning Data, San Diego, CA, Amer. Meteor. Soc., paper 2.3.

Petersen, W. A., H. J. Christian, and S. A. Rutledge, 2005: TRMM observations of the global relationship between ice water content and lightning. *Geophys. Res. Lett.*, 26 July 2005, **32;14**, L14819 doi: 10.1029/2005GL023236.

Skamarock, W. C., J. B. Klemp, J. Dudhia, D. O. Gill, D. M. Barker, M. G. Duda, X.-Y. Huang, W. Wang, and J. G. Powers, 2008: A description of the Advanced Research WRF Version 3. NCAR Technical Note NCAR/TN-475+STR, 123 pp.

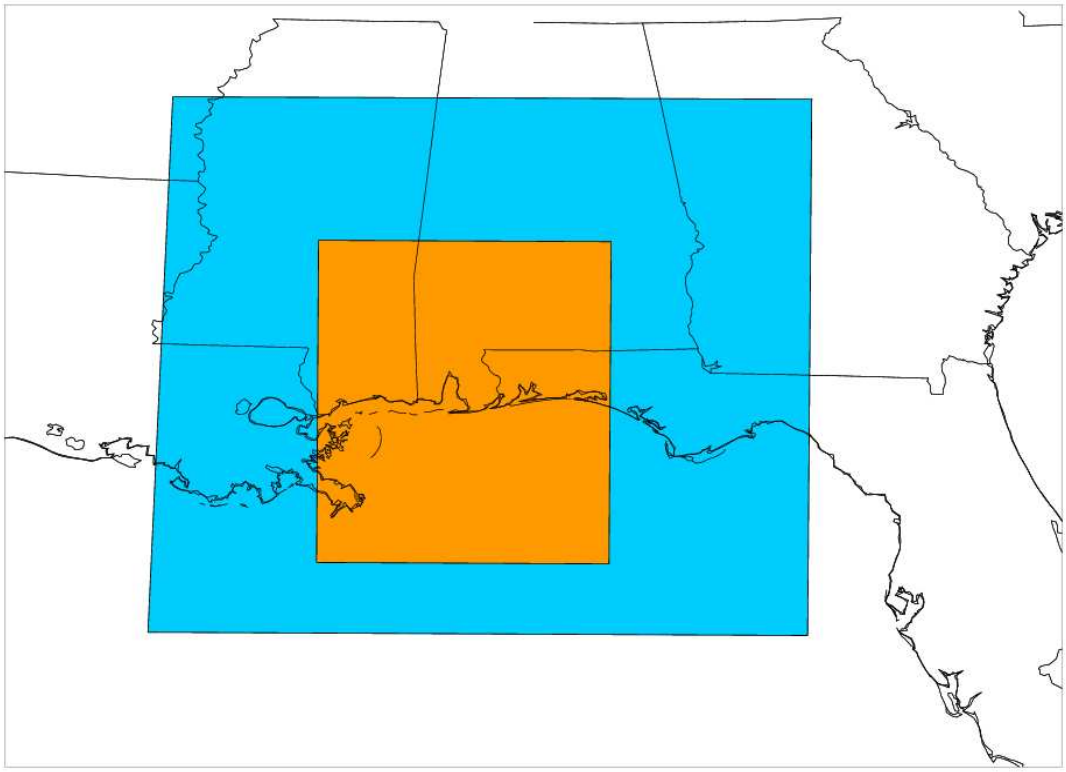

Fig. 1. Map showing outer (blue) and inner (orange) simulation domain, for MOB area experiments.

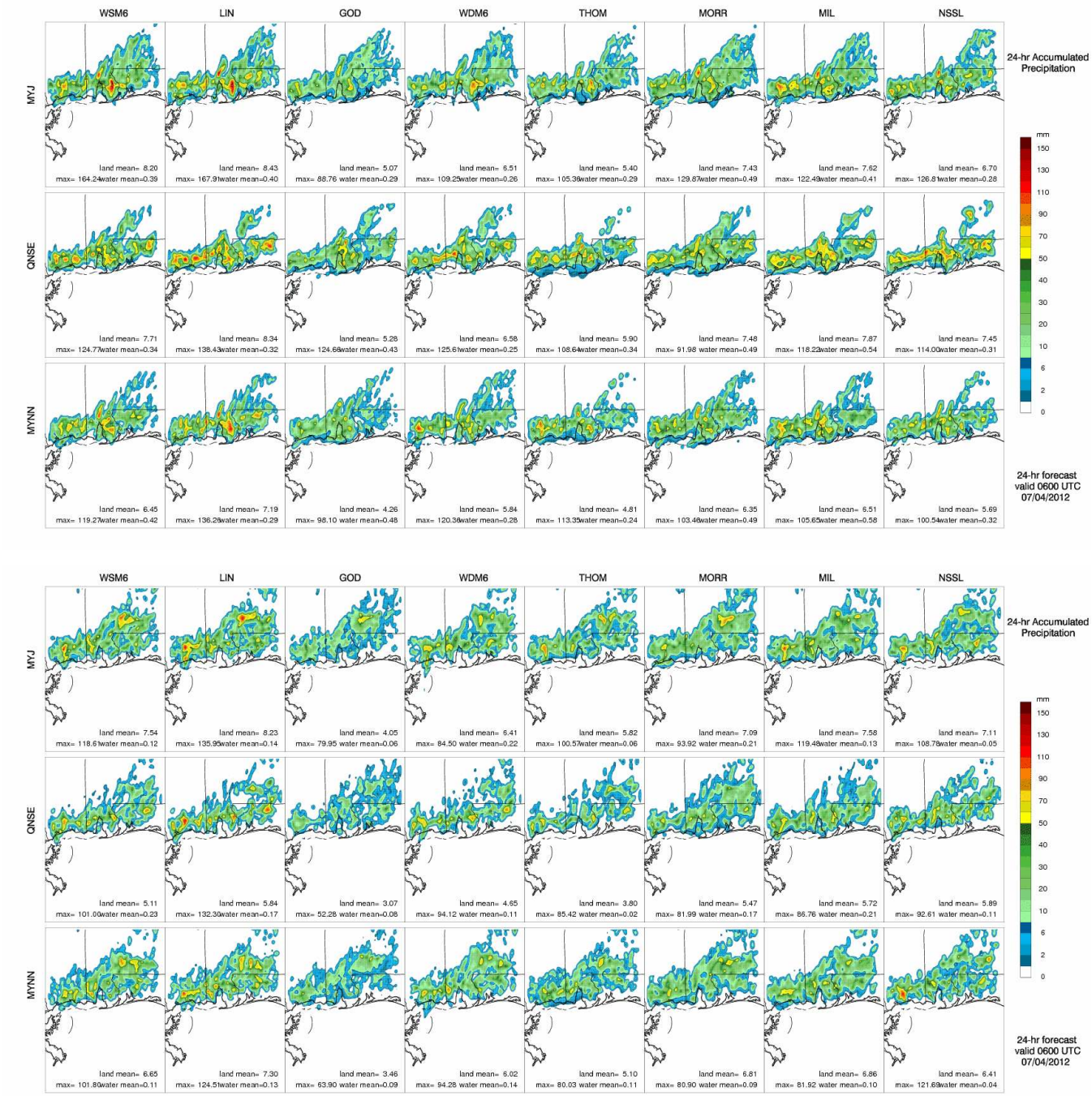

Fig. 2. Simulated total 24-h precipitation ending at 06 UTC 04 July 2012, for the MOB subdomain of Fig. 1. (a; top) from "control" simulations; (b; bottom) from "SPoRT" simulations; observations are provided in part (c), next page. Subdomain-wide maximum accumulations are printed on each plot panel of (a) and (b). Units are given in mm.

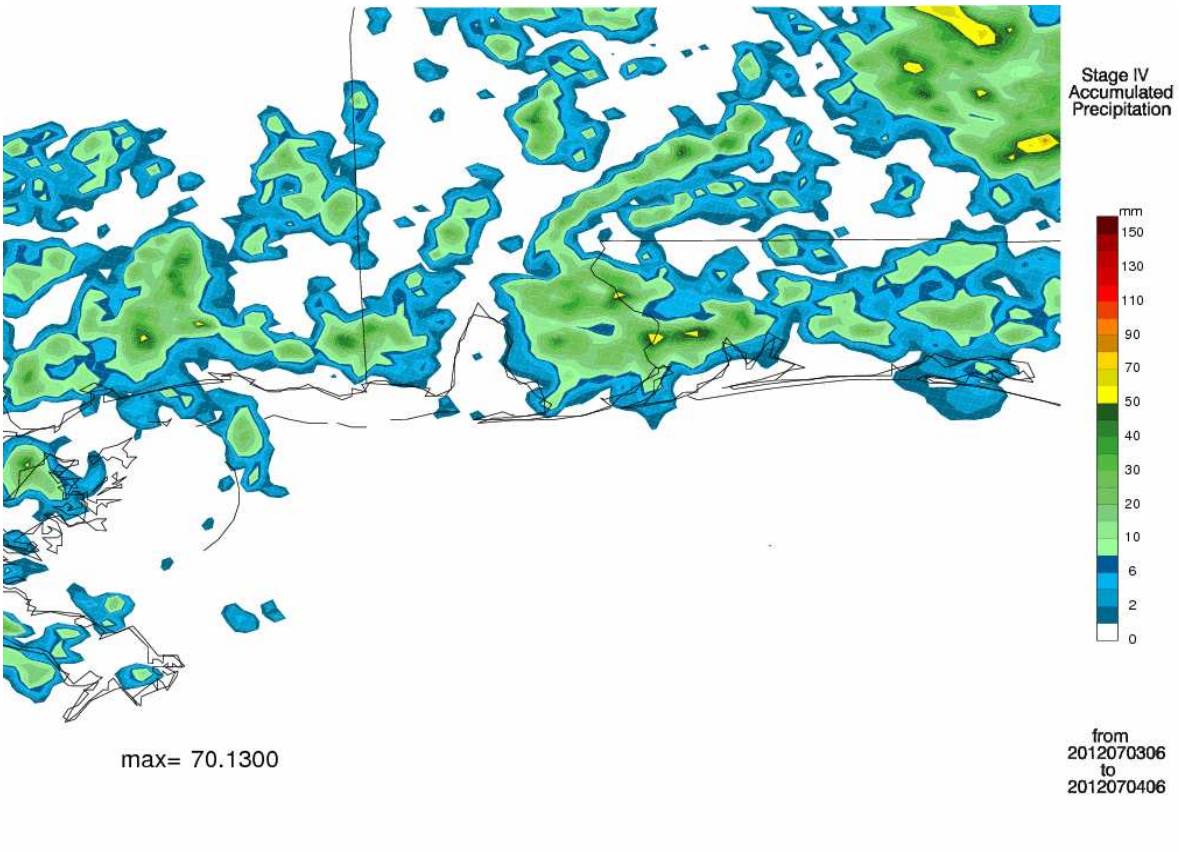

Fig. 2c. Observed 24-h precipitation ending at 06 UTC 04 July 2012, for the MOB subdomain of Fig. 1. Data are from Stage 4 observations. Subdomain-wide maximum accumulations are printed on the plot panel, with units in mm.

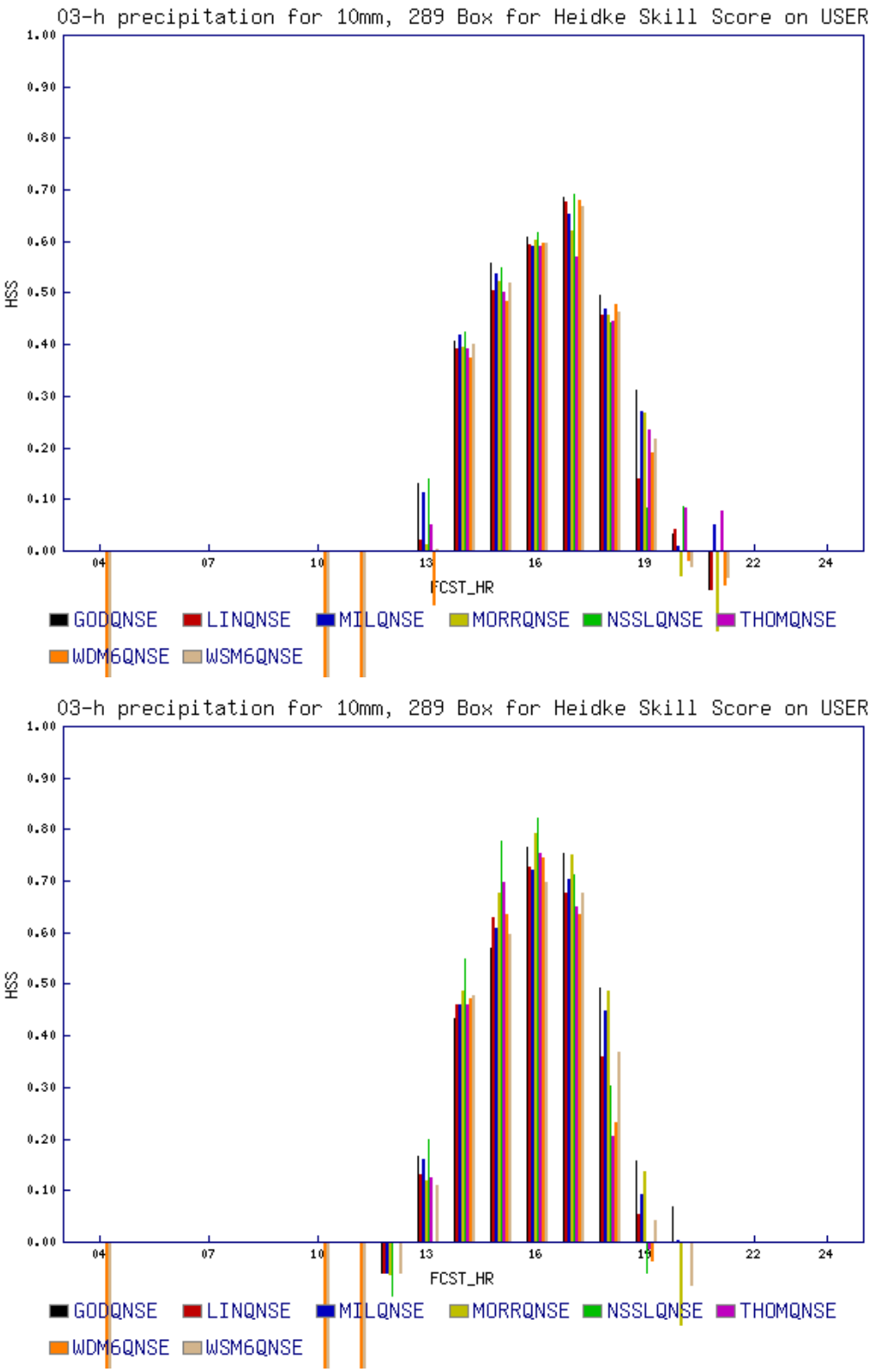

Fig. 3. Time-evolving precipitation Heidke Skill Scores for each of the eight QNSE microphysics choices for the 03 July 2012 storms at MOB. Legend describing the color codes for each scheme is provided at bottom. (a; top) Heidke scores for "control" simulations; (b; bottom) for "SPoRT" runs.

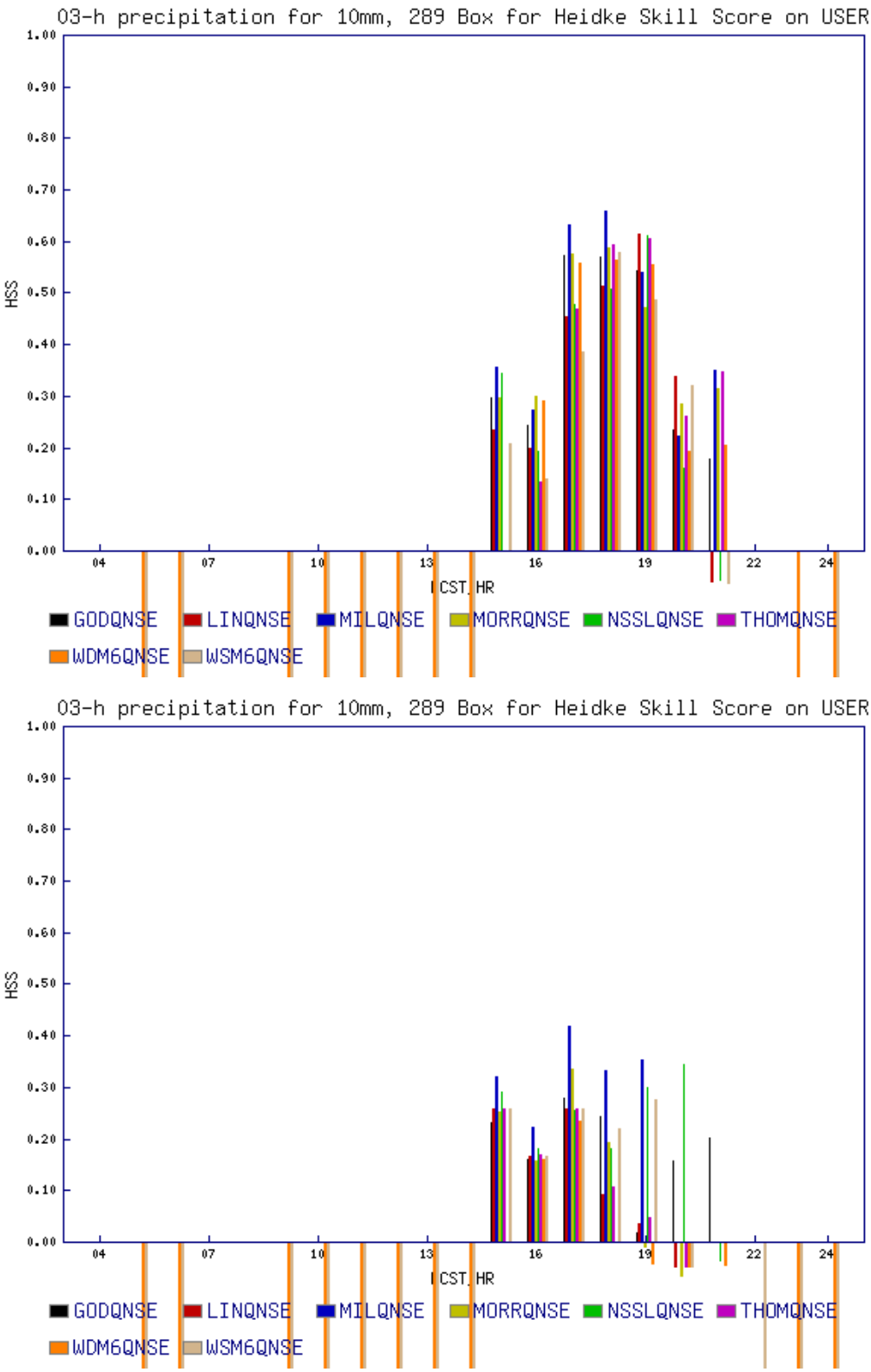

Fig. 4. As in Fig. 3, but for HGX subdomain. Note reduction of HSS values for the "SPoRT" runs during the period of active convection, in contrast to what was shown in Fig. 3.

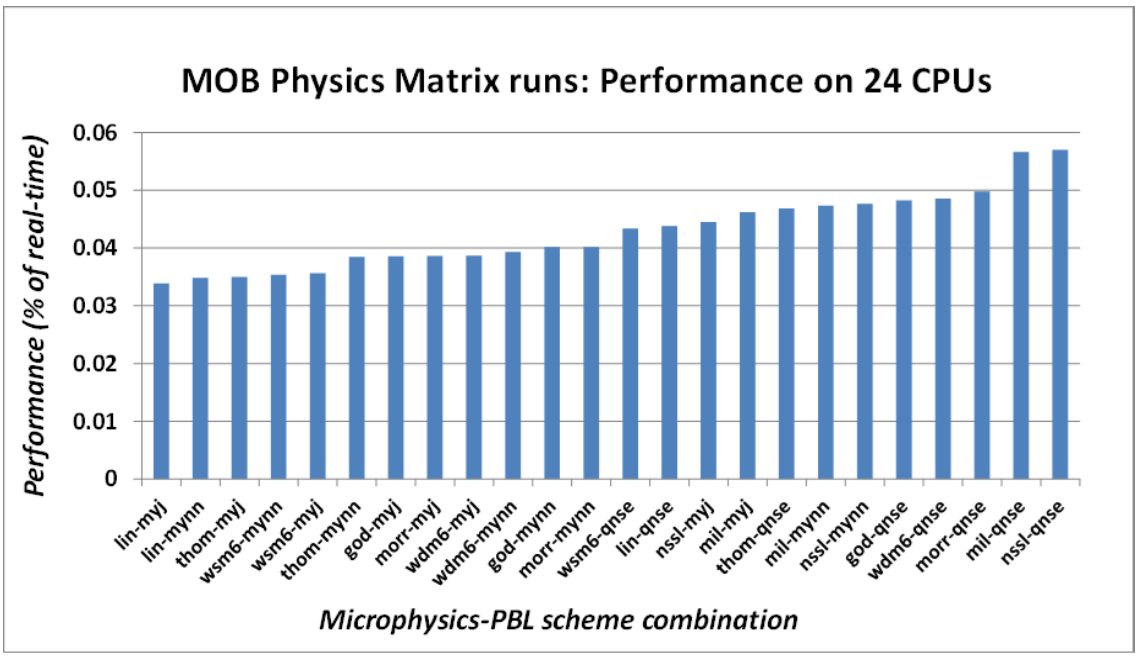

Fig. 5. Plot of run time data for each of the "control" MOB simulations of 3 July 2012. Results for "SPoRT" runs and HGX runs were roughly similar.